Biochimica et Biophysica Acta 1838 (2014) 784–792

Contents lists available at ScienceDirect

Biochimica et Biophysica Acta

journal homepage: www.elsevier.com/locate/bbamem

Architecture of the hepatitis C virus E1 glycoprotein transmembrane domain studied by NMR

Hadas Zazrin, Hadassa Shaked, Jordan H. Chill *

Department of Chemistry, Bar Ilan University, Ramat Gan 52900, Israel

ARTICLE INFO

Article history:
Received 7 May 2013
Received in revised form 24 October 2013
Accepted 28 October 2013
Available online 2 November 2013

Keywords:
Hepatitis C virus
Envelope glycoproteins
Nuclear magnetic resonance
Protein structure
Membrane-associated proteins
Transmembrane helix

ABSTRACT

Oligomerization of hepatitis C viral envelope proteins E1 and E2 is essential to virus fusion and assembly. Although interactions within the transmembrane (TM) domains of these glycoproteins have proven contributions to the E1/E2 heterodimerization process and consequent infectivity, there is little structural information on this entry mechanism. Here, as a first step towards our long-term goal of understanding the interaction between E1 and E2 TM-domains, we have expressed, purified and characterized E1-TM using structural biomolecular NMR methods. An MBP-fusion expression system yielded sufficient quantities of pure E1-TM, which was solubilized in two membrane-mimicking environments, SDS- and LPPG-micelles, affording samples amenable to NMR studies. Triple resonance assignment experiments and relaxation measurements provided information on the secondary structure and global fold of E1-TM in these environments. In SDS micelles E1-TM adopts a helical conformation, with helical stretches at residues 354–363 and 371–379 separated by a more flexible segment of residues 364–370. In LPPG micelles a helical conformation was observed for residues 354–377 with greater flexibility in the 366–367 dyad, suggesting LPPG provides a more native environment for the peptide. Replacement of key positively charged residue K370 with an alanine did not affect the secondary structure of E1-TM but did change the relative positioning within the micelle of the two helices. These results lay the foundation for structure determination of E1-TM and a molecular understanding of how E1-TM flexibility enhances its interaction with E2-TM during heterodimerization and membrane fusion.

1. Introduction

1.1. The hepatitis C virus

Hepatitis C virus (HCV) is the second most common chronic viral infection, estimated to afflict 3% of the world population, causing chronic hepatitis, cirrhosis, hepatic carcinomas as well as extra-hepatic diseases [1]. The HCV genome encodes a ~3000 amino-acid long polypeptide precursor which is later co- and post-translationally processed into at least 10 mature proteins [2]. Of these, the structured proteins, the core protein and envelope glycoproteins E1 and E2, form the viral particle, while the non-structured proteins are involved in the replication cycle and its regulation through protease, helicase and polymerase activities [3]. Despite progress in our understanding of HCV biology, improvements upon the only partially effective interferon/ribavirin treatment regimen, such as protease inhibitors, nucleoside inhibitors, and monoclonal antibodies, have been slow, and plagued by mediocre response levels and undesirable side-effects [4].

1.2. The E1/E2 heterodimer is critical to viral infectivity

E1 and E2 are both type I membrane proteins (MPs) each comprised of a large heavily glycosylated N-terminal ectodomain, a single membrane spanning domain and a short C-terminal cytoplasmic tail. The two glycoproteins assemble into a heterodimer which is the major component of the viral envelope and obligatory for viral infectivity [5]. Several studies have investigated the interaction mode between the two ectodomains and their contribution to the fusion process [6–8]. The E2 ectodomain is also known to recognize the host tetraspannin CD81 receptor, an important step en route to membrane fusion and viral entry [9,10], and anti-E2 antibodies are currently under investigation as HCV therapies [11]. However, study of the membrane-spanning (transmembrane, TM) domains has proven more challenging. It is known that besides directing and anchoring E1 and E2 to the endoplasmic reticulum and acting as signal sequences, these segments, E1-TM and E2-TM, are major contributors to the assembly of the E1-E2 heterodimer [12]. Mutational studies of the TM domains, each adopting α-helical conformations and ~30 amino acids long, identified structural elements

Abbreviations: CD, circular dichroism; CPMG, Carr–Purcell–Meiboom–Gil (pulse-train); DHPC, dihexanoylphosphatidylcholine; DPC, dodecyl-phosphocholine; DSS, 4,4-dimethyl-4-silapentane-1-sulfonic acid; DTT, 1,4-dithio-D-threitol; HCV, hepatitis C virus; HSQC, heteronuclear single-quantum coherence; IPTG, isopropyl β-D-1-thiogalactopyranoside; LPPG, 1-palmitoyl-2-hydroxy-sn-glycero-3-phospho-(1'-rac-glycerol); MBP, maltose-binding protein; MP, membrane-embedded protein; NMR, nuclear magnetic resonance; SDS, sodium dodecylsulphate; TEV, tobacco etch virus (protease); TM, transmembrane domain

* Corresponding author.
E-mail address: Jordan.Chill@biu.ac.il (J.H. Chill).

0005-2736/$ – see front matter © 2013 Elsevier B.V. All rights reserved.
http://dx.doi.org/10.1016/j.bbamem.2013.10.021

contributing to their association, a $G^{354}xxxG^{358}$ element at the extracellular side of E1-TM, and charged residues K^{370} on E1-TM, and D^{728} and R^{730} on E2-TM [13,14] (See Fig. 1). Mutations at these positions resulted in typical 3 to 4-fold reductions in heterodimer formation. In light of recent advances in targeting TM domains for drug discovery [15], a molecular understanding of dimerization in the membrane-embedded region of the E1/E2 heterodimer is of great interest.

1.3. Bitopic membrane proteins and their study by NMR

The TM-domains of the E1/E2 heterodimer form a bitopic system, an architecture which represents more than half of MPs in analyzed genomes [16]. This is an arrangement of two single-TM helical membrane spanning domains which assume a parallel orientation and associate within the membrane via non-covalent interactions. Several disease-causing mutations have been found in bitopic systems, highlighting their independent importance in both health and disease [17,18]. The interactions between membrane helical domains have drawn great interest because of their importance in folding, structure and stability in polytopic MPs, and because the association of two monotopic MPs is a paradigm of cellular signaling. As for all MPs, membrane helical segments challenge structural methods such as X-ray crystallography and nuclear magnetic resonance (NMR), since such peptides must be solubilized in a membrane-mimicking environment, greatly complicating sample preparation and data acquisition. Nevertheless, significant progress in the ability of NMR to address membrane-embedded peptides and bitopic MPs has been recently reported [19,20]. MPs can be studied using NMR by solubilization in micelles or disc-like bicelles formed by detergents or phospholipids [21–24] or assembled nano-discs [25], which serve as surrogate membranes and stabilize the protein in aqueous environment. Solution state NMR allows investigation in solution, an environment which closely mimics that of native MPs, and is sensitive to dynamic processes on a wide range of timescales unobservable using other methods [26,27]. In addition, several NMR-based methods are available for studying protein–protein interactions [27–30], including potentially weak (above μM affinity) interactions between TM domains [31,32], and NMR excels at studying the overall fold of proteins comprised of multiple locally rigid domains by analyzing their interactions and relative orientations [33].

Here we harness the abilities of solution NMR to provide a structural characterization of the E1-TM domain from the HCV envelope glycoprotein. Focusing on a membrane-spanning peptide solubilized in detergent and phospholipid micelles, we show it adopts a helical conformation under these conditions, with the length of the helical segments depending on the micelle composition. ^{15}N relaxation rates and measurements of solvent accessibility are utilized to characterize the architecture and biophysical behavior of the peptide embedded in the micelle. These findings lay the necessary foundations for a comprehensive study of interactions between transmembrane segments of E1/E2 en route to their association.

2. Materials and methods

2.1. Media and solvents

Custom synthesized DNA oligomers (primers) with codon usage optimized for *E. coli*, sodium dodecylsulphate (SDS), and Isogro-DCN supplement for triply labeled media were obtained from Sigma–Aldrich (St. Louis, MO, USA). Isotopically labeled chemicals for constructing labeling media, including $^{2}H_2O$, ^{13}C-labeled glucose and $^{15}NH_4Cl$, were purchased from Cambridge Isotope Laboratories (Andover, MA, USA). Dodecylphosphocholine (DPC) was purchased from Affymetrix (Maumee, OH, USA) and dihexanoylphosphatidylcholine (DHPC) and 1-palmitoyl-2-hydroxy-sn-glycero-3-phospho-(1′-rac-glycerol) (LPPG) were purchased from Avanti Polar Lipids, Inc. (Alabaster, AL, USA). M9 minimal media was made as previously described [34], with substitution of $^{15}NH_4Cl$, $^{13}C_6$-glucose and $^{2}H_2O$ for producing isotope-labeled E1-TM. HPLC grade solvents HCOOH and *iso*-C_3H_8OH were purchased from Biolabs (Jerusalem, Israel).

2.2. Cloning of the E1-TM sequence

The coding sequence for E1-TM (GeneArt, Regensburg, Germany) was inserted into a pETMBP-TEVH vector, a modified pET28a(+) construct containing the maltose binding protein (MBP) coding sequence [35], between the KpnI and XhoI restriction sites. This was accomplished by overlap extension using the polymerase chain reaction (PCR)-based restriction site-free cloning (RF-cloning) essentially as previously described [36]. In the first PCR, an E1-TM-carrying pET41a plasmid was incubated with primers E1-TM 5′ and E1-TM 3′ to amplify a double stranded DNA fragment that included the coding sequence for 33 E1 residues (351–383), flanked on either side by six additional amino acids to increase peptide solubility, and complementary sequences to pET-MBP-TEVH. This resulted in an E1-TM-encoding megaprimer which was carried over to the second stage. The second PCR utilized vector pET-MBP-TEVH as DNA template and the purified mega primer. The plasmid was amplified in *E. coli* DH5α cells. The DNA sequence of the obtained plasmid, referred to as pET-MBP-TEVH_E1, was confirmed by DNA sequencing. *E. coli* BL-21 competent cells were transformed with plasmid pET-MBP-TEVH_E1 for expression of a fusion protein comprised of 380 residues of MBP, a 17 residue linker containing a His_6-tag and a tobacco etch virus (TEV) protease cleavage site, the 45 residue DPEREK-(E1-TM)-EREKDP sequence, followed by a His_8-tag (Fig. 1). The K370A mutant was created using a QuikChange kit (Stratagene, Santa Clara, CA, USA).

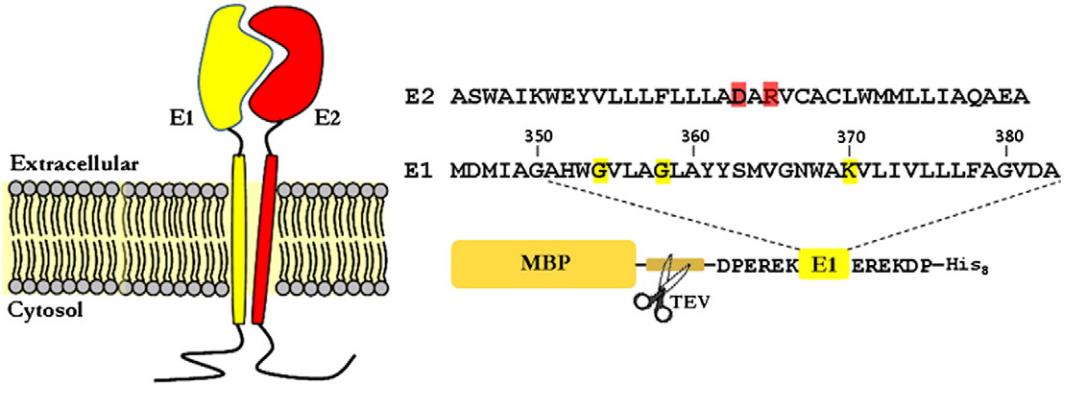

Fig. 1. The E1/E2 glycoprotein heterodimeric system in HCV. Left, schematic representation of the HCV E1 (yellow) and E2 (red) glycoproteins, emphasizing the segments embedded in the viral membrane. Right, membrane-spanning sequences of E1 (E2), with residues known to be involved in heterodimerization highlighted in yellow (red), and the E1-TM construct. Shown are the MBP carrier protein, TEV cleavage site, and the E1-TM segment employed in this study, including residues added for solubility enhancement.

2.3. Expression and purification of the E1-TM peptide

E1-TM was expressed in M9 minimal medium using previously described protocols [34]. ^{15}N- and ^{13}C-isotope labeling was achieved using 1 g/L 99% $^{15}NH_4Cl$ and 2.5 g/L 99% $^{13}C_6$-glucose, respectively. Briefly, *E. coli* BL21 cells were grown in M9 minimal media at 37 °C to an OD_{600} of 0.8, at which point isopropyl-thio-galactose (IPTG) was added to a final concentration of 1.0 mM and induction proceeded at 27 °C overnight. For preparation of deuterated samples, 200 mL of H_2O-based M9 culture was grown at 37 °C until the OD_{600} ~ 0.5 level was reached. Then, cells were gently spun down (1400 g, 20 minutes at ambient temperature) and resuspended in 1 L D_2O-based M9 culture supplemented with 1 g/L Isogro-DCN dry powder (Sigma–Aldrich, St, Louis, MO, USA). Then cells were grown again to the OD_{600} ~ 0.8 level, induced, and grown overnight at 27 °C. Cells were harvested by centrifugation and lysed by homogenization (C5 homogenizer, Avestin) in lysis buffer (20 mM NaPi, pH 7.4, 500 mM NaCl, 20 mM imidazole, 1 mM dithiothreitol (DTT)). The clarified lysate was applied on a HiTrap Chelating HP column (GE Healthcare, Uppsala, Sweden.) charged with Ni^{2+}. The column was washed with several column volumes of lysis buffer, and bound protein was then eluted by raising the imidazole concentration to 500 mM. The elute was dialyzed for 12–14 h at 25 °C against TEV protease cleavage buffer (20 mM NaPi, pH 7.5, 150 NaCl and 1 mM DTT), and later incubated with TEV protease (1:10 w\w) for 5 h at 30 °C, resulting in quantitative cleavage of the E1-TM peptide from its MBP carrier. The E1-TM peptide was purified by RP-HPLC (Young-Lin, Kyounggido, Republic of Korea) using a preparative C4 column (Phenomenex, Torrance, CA, USA) at 60 °C and a H_2O:isopropanol linear gradient (30:70 to 50:50) containing 10% (v/v) formic acid. Fractions containing E1-TM were pooled and lyophilized, after which they could be solubilized in detergent for NMR experiments. Protein concentration was determined by measuring the absorbance at 280 nm, based on a specific absorbance of 2.2 OD_{280} for a 1 mg/mL solution.

2.4. Circular dichroism measurements

CD experiments were acquired on a Chirascan polarimeter (Applied Photophysics, Surrey, United Kingdom) for a 15 μM samples of E1-TM peptide solubilized in SDS, LPPG, or DPC, in 20 mM NaPi buffer, pH 6.5. Typical detergent:peptide molar ratios were 600–1500:1 to ensure single occupancy of micelles by the peptide. Samples were placed in a 1 mm cuvette and the 180–260 nm range was scanned in 0.5 nm steps with a bandwidth of 2 nm. Each experiment was repeated three times and subtracted from a measurement of an identical buffer sample. Results were analyzed using the CDSSTR module of the DichroWeb platform for the 190–240 nm range[37].

2.5. NMR spectroscopy

All 2D- and 3D-NMR measurements were conducted on a DRX700 Bruker (Bruker BioSpin, Karlsruhe, Germany) spectrometer using a cryogenic triple-resonance TCI probehead equipped with z-axis pulsed field gradients. NMR samples containing 0.3–0.6 mM E1-TM (wildtype or K370A mutant) were prepared in 20 mM phosphate buffer, with pH values of 6.0–6.5, 20 mM NaCl, 7% ^2H_2O, and an appropriate detergent, and placed in a 5 mm Shigemi (Shigemi, Allison, PA, USA) or Wilmad (Wilmad Labglass, Vineland, NJ, USA) NMR tube. Measurements were conducted at 318 K. Transverse relaxation-optimized (TROSY) ^1H,^{15}N-HSQC experiments (tr-HSQC) for screening of measurement conditions were acquired using a standard sequence run for 30–60 min. For backbone assignment, TROSY-based triple resonance HNCO, HNCA, HN(CO)CACB, and HNCACB experiments using sensitivity-enhanced echo-antiecho detection [38] were acquired for partially deuterated, uniformly ^{13}C,^{15}N-labeled E1-TM. All triple-resonance experiments were typically acquired with 32–36 complex points and an acquisition time of 20.2–22.8 ms in the ^{15}N dimension, and 512 complex points and an acquisition time of 52.2 ms in the observed dimension. In the ^{13}C dimension, experiments with ^{13}CO ($^{13}C^{\alpha}$) evolution were acquired with 32–40 complex points and 21.2–26.5 (7–7.5) ms acquisition time, and experiments with $^{13}C^{\alpha/\beta}$ evolution were acquired with 56–64 complex points and 5.3–6.1 ms acquisition time. All spectra were processed using the TopSpin 2.1 package (Bruker BioSpin, Karlsruhe, Germany). Chemical shifts were referenced indirectly against 4,4-dimethyl-4-silapentane-1-sulfonic acid (DSS).

Relaxation measurements were conducted in scan-by-scan interleaved fashion with a tr-HSQC spectrum for readout at static magnetic field of 16.4 T and 318 K. To ensure sufficient resolution in the 2D spectrum, acquisition times were set to 104.5 ms and 58–70 ms in the ^1H- and ^{15}N-dimensions, respectively. Longitudinal relaxation rates (R_1) were estimated from a series of decay spectra with delays of 2 (reference spectrum), 152, 302, 502, 702, 902, and 1202 ms. Similarly, transverse relaxation rates (R_2) were estimated from a series of decay spectra using a Carr–Purcell–Meiboom–Gil (CPMG) relaxation block with delays of 16.96 (reference spectrum), 33.92, 50.88, 67.84, 84.80, 101.76, and 135.68 ms. The heteronuclear ^{15}N-{^1H}-NOEs (hetNOEs) were determined by recording pairs of interleaved spectra with and without proton saturation during the recycle delay [39,40]. A total of 16 transients were collected per t_1 experiment and delays between scans were 3.0 s. Total experiment time for each relaxation measurement was 42–48 h. In both cases intensities were fit to an exponential decay function using the Bruker TopSpin 2.1 Dynamics suite, and hetNOEs were derived from the intensity ratio in reference and attenuated spectra.

3. Results

3.1. Design and biosynthesis of the E1-TM peptide

Due to their hydrophobicity, TM domains are notoriously difficult to prepare using solid-phase synthesis methods. We therefore set out to express E1-TM using a fusion protein system. The E1 sequence was chosen from a consensus sequence of viral strains. Several studies have focused on the location of the membrane-spanning domain of the E1 glycoprotein, with a general agreement that residues 353 to 383 should include this domain [41–43]. A recent study utilized multiple bioinformatics tools to further pinpoint the location of the hydrophobic stretch of residues traversing the membrane, suggesting this region to span residues 354–379 [44], in agreement with earlier predictions [14]. Therefore, we chose a 33-residue segment of E1 (A^{351}HWGVLAGLAYYSM VGNWAKVLIVLLLFAGVDA^{383}), to which we added a hexa-residue peptide on either side (DPEREK and EREKDP at the N- and C-terminii, respectively) in order to increase its solubility (Fig. 1). The alternatingly charged residues were chosen to increase solubility in water without affecting the overall electrostatic properties of the peptide. The resulting polypeptide was fused to MBP [45] via a TEV protease cleavage site. This 50 kDa protein (including the His_8-tag) could be expressed as a soluble polypeptide, presumably due to the ability of MBP to stabilize the hydrophobic E1-TM and preclude aggregation. SDS-PAGE analysis showed TEV cleavage to be complete, but E1-TM remained bound to the fusion protein as evidenced by size exclusion chromatography. Due to their different hydrophobic character, the desired TM peptide could be separated from the fusion protein by RP-HPLC on a C4 column at strongly acidic conditions (10% HCOOH, 60 °C) and a H_2O: isopropanol gradient (Supporting Information, Fig. S1). Lyophilized E1-TM could then be solubilized in a detergent of choice in preparation for NMR and CD experiments.

3.2. Characterization and resonance assignment of E1-TM

The choice of detergent for solubilization of membrane peptides is known to have far-reaching consequences on the ability to study their structure using NMR as well as the biological interpretation of these

results [22,24,46,47]. We therefore prepared samples of E1-TM solubilized by four different detergents and phospholipids, sodium dodecylsulphate (SDS), dodecylphosphocholine (DPC), dihexanoylphosphatidylcholine (DHPC) and 1-palmitoyl-2-hydroxy-sn-glycero-3-phospho-(1′-rac-glycerol) (LPPG). Initial characterization of these samples was performed using circular dichroism (CD). The SDS- and LPPG-solubilized E1-TM produced CD curves with the characteristic minima at 208 and 222 nm, indicating the prevalence of α-helical secondary structure in the detergent-solubilized peptides. Notably, the LPPG sample appeared to contain more helical character than the SDS sample. In contrast, in DPC and DHPC E1-TM exhibited considerably less secondary structure, suggesting it was not properly stabilized in native form at these conditions (Fig. 2A). Using the DichroWeb CDSSTR module [37] we determined that the proportion of helical (β-sheet) character in E1-TM was 38 (13), 51 (9), 28 (26) and 14 (33) % in SDS, LPPG, DPC and DHPC, respectively (Table 1). CD curves were insensitive to changes in temperature in the 298–318 K range.

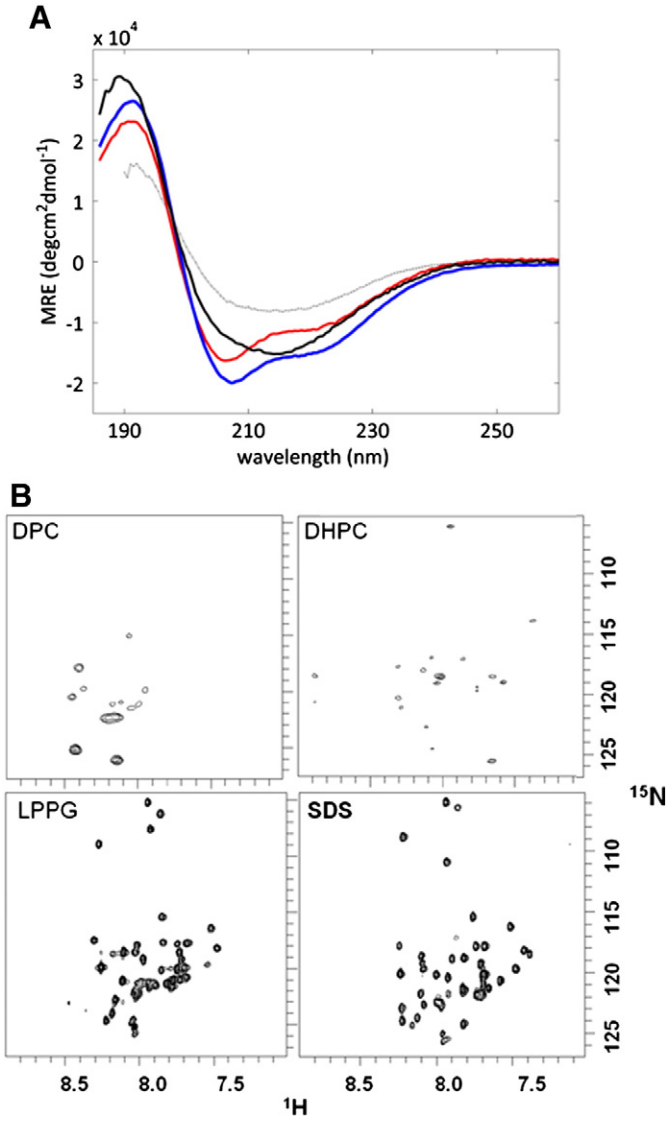

Fig. 2. Characterization of E1-TM in various membrane-mimicking environments. Biophysical behavior of E1-TM was characterized in various detergents and phospholipids. A) Circular dichroism curves of E1-TM solubilized in 40 mM SDS (red), 40 mM LPPG (blue), 40 mM DPC (black) and 30 mM DHPC (grey). (B) tr-^{1}H–^{15}N-HSQC spectra of 0.6 mM E1-TM solubilized in various detergents were used to characterize the samples and optimize measurement conditions. All were acquired for detergent-solubilized E1-TM in 20 mM NaCl, 20 mM phosphate buffer at pH 6.7, and at a field strength of 16.4 T and a temperature of 318 K. Shown from the upper left corner in clockwise fashion are spectra in DPC, DHPC, SDS and LPPG.

We continued this characterization by comparing tr-^{1}H,^{15}N-HSQC spectra of these four samples. This demonstrated that detergents with negatively charged headgroups, SDS and LPPG, are suitable for studying E1-TM. Although both spectra exhibited low spectral resolution characteristic of helical membrane segments, 41 (in SDS) and 43 (in LPPG) crosspeaks were observed, close to the number expected for E1-TM. In contrast, both phosphocholine detergents afforded low-quality spectra with limited signal-to-noise and several absent cross-peaks (Fig. 2B). Specifically, none of the expected four cross-peaks arising from Gly residues could be observed in these detergents, whereas SDS- and LPPG-solubilized samples exhibited all such peaks. As E1-TM is predicted to be a helical membrane-spanning peptide, this is consistent with the higher helical contents found by CD in SDS and LPPG.

SDS and LPPG are located on opposite ends of the range of detergents suitable for structural NMR of membrane peptides. SDS assembles into smaller micelles [46], resulting in improved linewidths, and while it will stabilize the membrane-embedded residues, its strongly charged headgroup and relatively short aliphatic tail often force peptides to adopt less-than-native conformations. In contrast, the more biological nature of the LPPG headgroup and its longer fatty acid chain make LPPG micelles a useful and NMR-amenable membrane-mimicking environment [22], even though relaxation losses for the larger micellar assembly may be of some consequence. Thus, we proceeded to prepare triply [^{2}H,^{13}C,^{15}N]-labeled E1-TM samples solubilized in SDS and LPPG micelles in order to compare the conformations adopted by the peptide in the two environments.

3.3. Secondary structure of E1-TM in detergent and phospholipid micelles

Backbone resonances were assigned for the E1-TM peptide solubilized in SDS and LPPG micelles using a combination of TROSY versions of the HNCO, HN(CA)CO, HNCA, HNCOCACB, and HNCACB experiments [38]. While spectra obtained in both micelles exhibit relatively poor spectral dispersion which is characteristic of helical membrane segments, the above experiments were sufficient to assign the majority of backbone residues. Fig. 3 displays sample strip plots demonstrating the connectivities established between adjacent residues as derived from the triple-resonance tr-HN(CA)CO and tr-HNCA experiments, and the fully-assigned HSQC spectrum for the LPPG-solubilized sample. The resonance assignment of E1-TM solubilized in SDS and LPPG micelles has been deposited in the Biological Magnetic Resonance Data Bank (BMRB), under accession code 19517. Differences between the fingerprint spectra and backbone chemical shifts in SDS (Supporting Information, Fig. S2) and LPPG (Fig. 3) indicated that the peptide adopted a characteristic conformation in each of the two micelles. Analysis of $^{13}C'$, $^{13}C^{\alpha}$, and $^{13}C^{\beta}$ secondary chemical shifts [48] in SDS (assignment level of 85% for ^{1}H–^{15}N pairs and 84% for backbone ^{13}C nuclei) showed that within the membrane domain E1-TM adopted a helical conformation, with helices spanning residues 354–363 (H1) and 371–379 (H2) connected by a 7-residue segment (364–370) in random coil conformation (Fig. 4). Residues 380–382 at the micelle–solution interface could not be observed, presumably lost to exchange-broadening which may result from hydrophobic mismatch between the peptide and the SDS

Table 1
Secondary structure in E1-TM.

	%sheet (CD)[a]	%helix (CD)[a]	%helix (NMR)[b]
SDS	13	38	36
LPPG	9	51	45
DPC	26	28	ND[c]
DHPC	33	14	ND[c]

[a] As determined by the CDSSTR module of the DichroWeb platform (ref. [37]).
[b] As determined by δ2D analysis of chemical shifts (ref. [48]).
[c] Not determined.

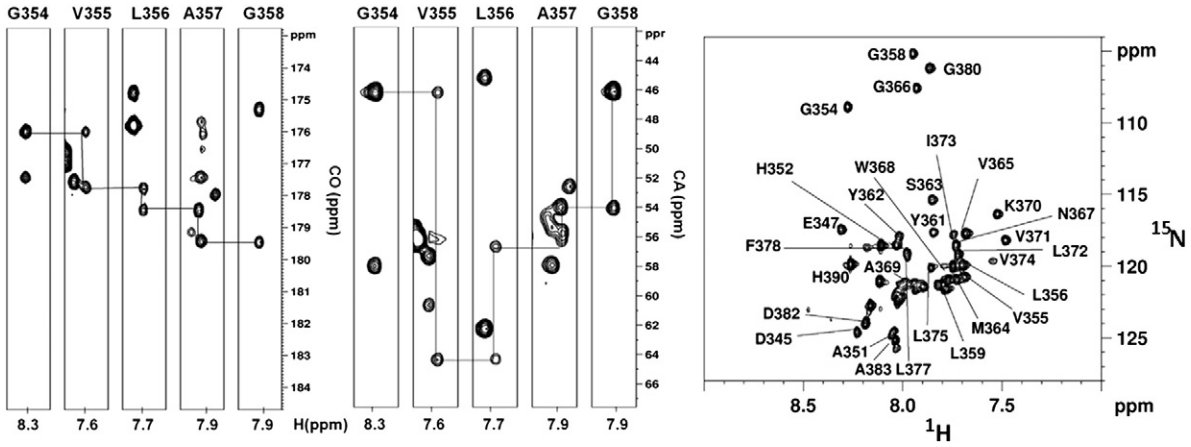

Fig. 3. Backbone assignment of E1-TM. Left, Strip plots derived from the tr-HNCA and tr-HN(CA)CO spectra of LPPG-solubilized E1-TM demonstrating the 'backbone-walk' which made possible the assignment of chemical shifts for residues 354–358 of the GxxxG motif. Right, The fully assigned tr-HSQC spectrum of E1-TM in LPPG micelles.

micelle. By comparison, E1-TM appeared to adopt a more helical conformation in LPPG micelles (assignment level of 97% for $^{1}H–^{15}N$ pairs and 95% for backbone ^{13}C nuclei). Here a helical conformation was observed throughout E1-TM, spanning residues 354–377. Residues G366 and N367 exhibited lower helical propensity, suggesting this dyad embodies a more flexible region within the helix. Significantly, residues 380–383 were now clearly visible, testifying to the fact that E1-TM is better stabilized by the long-chain and more biologically relevant LPPG. Helical content of E1-TM determined by secondary chemical shift analysis, 19 of 53 residues, or 36%, for SDS, and 24 of 53 residues, or 45%, for LPPG, were in reasonable agreement with the previously mentioned CD results (38 and 51%, respectively, Table 1).

3.4. Characterization of the E1-TM/LPPG macroassembly

We further probed the architecture of the E1-TM-containing LPPG micelle by measuring ^{15}N relaxation rates, a reliable reporter on backbone dynamics on the ps-ns timescale [39,49], and solvent accessibility of $^{1}H–^{15}N$ amide moieties, along the E1-TM backbone. R_1 and R_2 rates and hetNOEs were measured for LPPG-solubilized E1-TM at 318 K and 16.4 T. Elevated R_1 values (1.2–1.4 s^{-1}) and reduced R_2 and hetNOE values (5–7 s^{-1} and 0.4–0.5, respectively) were seen for residues 350–353 and 380–383, indicating that these segments are more flexible and therefore reside outside of the LPPG micelle. In contrast, the lower R_1 values (0.85–1.0 s^{-1}) and increased R_2 and hetNOE values (15–20 s^{-1} and 0.7–0.8, respectively) observed for residues 354–379 are characteristic of a more rigid domain, and unambiguously define the membrane-spanning region of the peptide (Fig. 5A–C). Residues N367, W368 and A369 differ in their relaxation parameters (higher R_1, lower R_2) in comparison to the entire membrane-spanning domain, confirming them as comprising a more flexible linker between structural elements. The ratio R_2/R_1 in the helical regions lies in the 18 to 20 range, predicting a global tumbling time of ~12 ns for the E1-TM-containing micelle at 318 K, which, based on the Stokes–Einstein equation for rotational diffusion of a spherical body, corresponds to a molecular weight of ca. 70 kDa. This is consistent with the known size of LPPG micelles, determined to be ~64 kDa [50], and the mass of E1-TM, slightly over 6 kDa.

Close examination of the R_2/R_1 ratios in the E1-TM hydrophobic domain distinguishes between relaxational behavior of H1 and H2 (Fig. 5D). The GVALG motif in H1 (residues 354–358) exhibits a lower R_2/R_1 ratio of 14 (range 12–15), others H1 residues (359–366) exhibit a higher ratio, 18 (range 17.3–20.1), whereas H2 (residues 371–378)

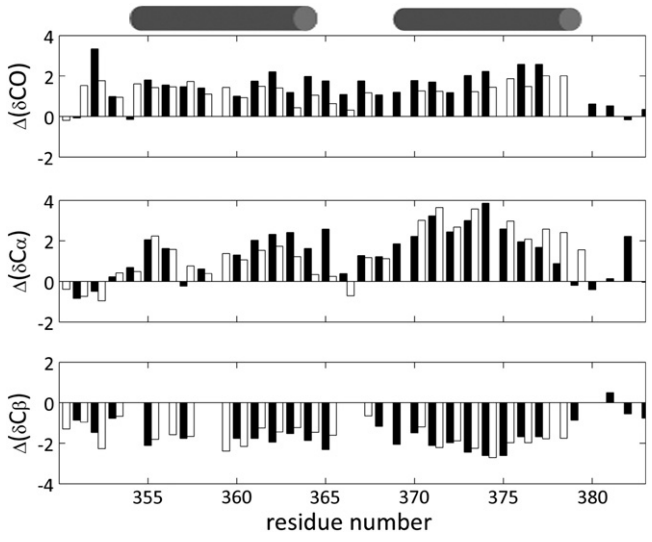

Fig. 4. Secondary chemical shifts of E1-TM define its fold. Secondary chemical shifts measured along the E1-TM backbone. Shown are values for $^{13}C'$ (top), $^{13}C^{\alpha}$ (middle) and $^{13}C^{\beta}$ (bottom) nuclei in SDS (empty bars) and LPPG (filled bars), respectively. The H1, H2 segments are designated by cylinders above the figure.

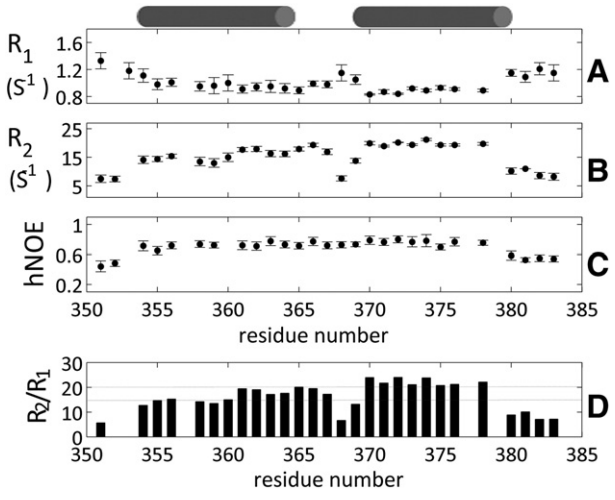

Fig. 5. Relaxation measurements report on ps-ns dynamics of the E1-TM-LPPG assembly. Backbone ^{15}N relaxation rates measured for $^{2}H,^{13}C,^{15}N$-labeled E1-TM at a static field of 16.4 T and 318 K. Shown are relaxation rates (A) longitudinal relaxation R_1, (B) transverse relaxation R_2, and (C) the heteronuclear ^{15}N-{^{1}H}-NOE. Typical errors in relaxation rate measurements (shown in error bars) were 3–5%. (D) The R_2/R_1 ratio is plotted against the E1-TM sequence, with the $R_2/R_1 = 15$ and $R_2/R_1 = 20$ levels marked in dotted lines. The H1, H2 segments are designated by cylinders above the figure.

exhibits the most elevated ratios, 22 (range 20.7–24). The statistically significant differences observed can be a reflection upon E1-TM structure as well as backbone motions. Based on the well-established influence of rotational diffusion anisotropy upon ^{15}N relaxation rates [51,52], this finding could indicate that the LPPG-solubilized E1-TM assembly is ellipsoidal, and that two helical domains are not co-linear. Alternatively, increased internal backbone motions on the ps-ns timescale of H1 could also result in lower R_2/R_1 ratios for the former region.

To further characterize the behavior of E1-TM in its solubilizing micelle, the accessibility of its amide protons to the bulk solvent was measured. E1-TM was dissolved in ^2H_2O-based buffer containing either SDS or LPPG micelles, resulting in residue-dependent loss of tr-HSQC signal as a function of solvent exposure. Spectra acquired for E1-TM solubilized in either SDS or LPPG micelles 30 min after exposure to deuterated buffer displayed only cross-peaks from the H2 helix, whereas cross-peaks from the H1 region or more flexible segments were not visible (Fig. 6). Based on theoretical calculations [53], this represents a protection factor of $>10^4$ for the H2 helix. Since the hetNOE values of both helices are very similar, and considering their hydrophobic nature, it is unlikely that the H1 is solvent exposed. We suggest that the presence of two glycine residues in the H1 helix increases the conformational flexibility and decreases expected protection factors. In addition, residues carrying labile protons (Y361, Y362, S363) may localize the H1 helix further from the micelle core, increasing the availability of solvent for exchange. Juxtaposed with the lower R_2 values observed in H1, we conclude that the two helices differ in the degree of internal backbone motion they experience.

3.5. Effects of the K370A mutation

Due to its known role in heterodimerization [14], and furthermore because of its anomalous placement as a charged residue within the lipophilic membrane, residue K370 presents a particularly intriguing aspect of LPPG-solubilized E1-TM. Having located the more flexible region of the helix in the vicinity of K370, we suspected that the charged nature of this residue may distort the membrane-spanning helix. To test this hypothesis, we mutated K370 into the hydrophobic and helix-promoting alanine residue, and re-assigned the backbone resonances by examination of the HNCACB spectrum and comparison to the assignment of wildtype E1-TM. Most significant changes in the tr-HSQC spectrum were observed as expected for K370 and neighboring residues A369 and V371, as well as non-neighboring residues G366 and V374 (Fig. 7A, C), presumably because these are positioned by the helical structure in proximity to the mutated residue. Smaller changes were exhibited by more distant residues, creating a distinct 'ripple' effect. The emerging pattern is that residues in both H1 and H2 are affected, and those exhibiting more significant effects are located on the same surface of the helical segments. This suggests that the position of the peptide within the stabilizing micelle is modified for the K370A mutant. However, the Lys-to-Ala mutation did not have a significant effect on secondary chemical shifts of E1-TM. Secondary chemical shifts were essentially comparable in the wildtype and mutant peptides, and, notably, no change was observed in the more flexible region, suggesting that a significant alteration of secondary structure did not occur (Fig. 7B). We conclude that neutralization of the K370 charge is not the dominating cause of structural changes accompanying the E1/E2 heterodimerization event.

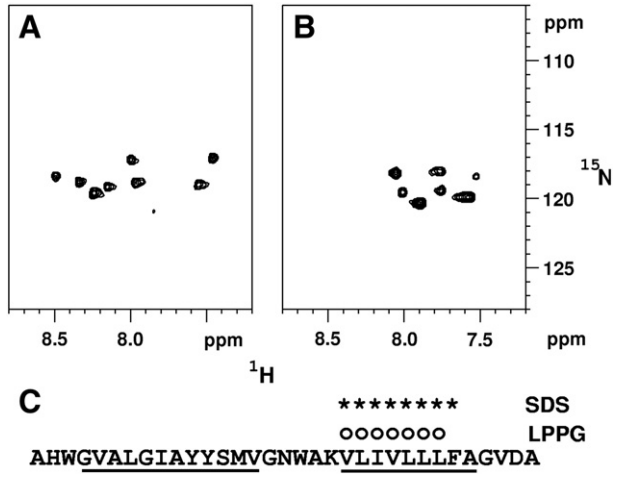

Fig. 6. Solvent accessibility of E1-TM in SDS and LPPG micelles. tr-^1H–^{15}N-HSQC spectra at 16.4 T and 318 K of 0.15 mM E1-TM solubilized in (A) SDS or (B) LPPG micelles 30 min after dissolution in ^2H_2O-based buffer containing 20 mM NaCl and 20 mM phosphate buffer. Only residues protected from solvent exchange are observed in such an experiment. (C) E1 amide groups protected from exchange are shown for SDS (asterisks) and LPPG (open circles).

4. Discussion

Heterodimerization of the E1/E2 glycoproteins has been shown to be a mandatory step for fusion of viral and host cell membranes during infection by HCV [5,12,14]. Both the extracellular domains and membrane-spanning helices of these glycoproteins contribute to this cellular event, as determined by the effects of mutations located within the hydrophobic membrane domains, E1-TM and E2-TM, upon viral infectivity. Thus, inhibition of the interaction between the two TM-domains is a promising avenue for combating HCV infection. The E1-TM/E2-TM complex forms a bitopic membrane system, consisting of two parallel α-helical segments with non-covalent interactions between them. Although typically these interactions are hydrophobic in nature, E1- and E2-TM uncharacteristically have charged residues embedded within the membrane, suggesting an electrostatic interaction which increases in importance in the hydrophobic membrane environment.

The current lack of structural information for E1- and E2-TM was the primary motivation for this study. However, synthesis of membrane-embedded peptides by chemical or recombinant methods is very challenging, since their strong aggregation tendency often frustrates such attempts at the level of expression or purification [54], and this hurdle needed to be overcome as a prerequisite for any structural study of E1/E2. We achieved this aim by fusing the E1-TM peptide via a linker containing a proteolysis cleavage site to the MBP C-terminus. The hydrophobic interaction between MBP and E1-TM which precludes peptide aggregation during expression persists after cleavage, as MBP and E1-TM co-eluted under normal conditions in size-exclusion chromatography. Separation by HPLC then yielded a pure E1-TM peptide. A second modification, addition of short flexible charged peptide segments at the two E1-TM terminii, contributed as well to the solubility of E1-TM, making HPLC elution possible as well as future phospholipid solubilization. Together these factors allowed a first preparation of E1-TM samples in membrane-mimicking environment amenable to structural study. Both SDS- and LPPG-based micelles produced E1-TM assemblies with stable conformations as judged by their fingerprint tr-^1H–^{15}N-HSQC spectra. Of these two surfactants, LPPG is well-known for its proven ability to stabilize MPs for several weeks while providing a close-to-native environment for the protein during acquisition of NMR data [22].

A combination of well-established NMR methods was employed to characterize the assembly of E1-TM within the stabilizing micelles in terms of micellar size and arrangement of the peptide within the micelle. An analysis of secondary chemical shifts showed E1-TM to adopt different conformations in the two micelles. In SDS micelles, E1-TM adopted a helix–linker–helix architecture, with helical segments including residues 354–363 and 371–379, while the intermediate segment exhibited chemical shifts inconsistent with a helical conformation. In contrast, solubilization in LPPG micelles resulted in a more helical E1-TM, consistent with the CD results. Specifically, a helical conformation was observed for residues 354–377, with decreased helical population values seen for the 366–367 dyad indicating the location of a potential

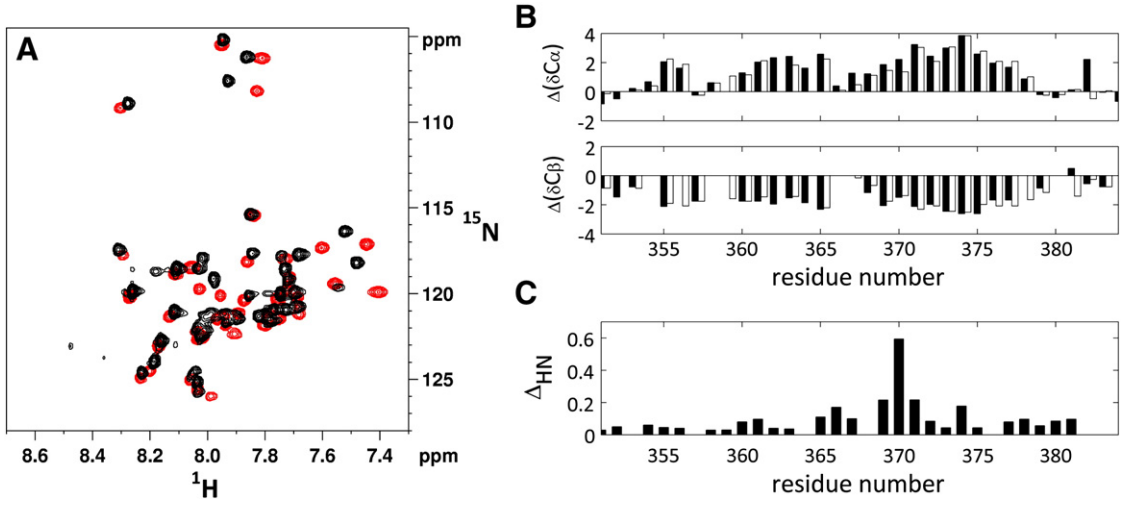

Fig. 7. Effects of the membrane-embedded K370 on E1-TM structure. (A) Comparison of fingerprint ^{15}N,^{1}H-tr-HSQC spectra for wildtype (black) and K370A mutant (red) E1-TM peptides. Residues with shifted resonances experience a change in chemical environment upon substitution of Ala for K370. (B) Secondary chemical shifts for $^{13}C^{\alpha}$ and $^{13}C^{\beta}$ nuclei of wildtype (filled bars) and K370A mutant (empty bars) E1-TM. (C) Chemical shifts changes induced along the E1-TM sequence by the K370A mutation, expressed as $\Delta_{HN} = (\Delta_H^2 + (\Delta_N/5)^2)^{1/2}$, where Δ_H and Δ_N are the individual change in ^{1}H and ^{15}N shifts, respectively.

kink in the helix. ^{15}N relaxation rates were consistent with the notion that residues 366–369 were more flexible in comparison to other E1-TM residues in the membrane-spanning domain. Occurrence of a kink in the vicinity of residue N367 is consistent with earlier studies identifying Asn residues as a common helix-breaking residue in TM-domain, a fact attributable to its polar sidechain which competes for hydrogen bonding with the backbone amides. Indeed, the kink in E1-TM was predicted by the TMKink server [55]. The difference between SDS- and LPPG-solubilized E1-TM appears consistent with micellar size. Thus, the larger LPPG micelle is capable of fully accommodating a helical E1-TM, whereas the smaller SDS micelle causes a curvature effect which kinks the peptide at the point most structurally amenable to such a conformation. We note that bicelles formed by a mixture of short- and long-chain phospholipids are recognized as a more natural environment for MPs because their shape resembles the native bilayer and they are less prone to curvature effects [46,56]. While a study in bicelles would be useful to verify our conclusions regarding E1-TM secondary structure, the estimated diameter of an LPPG micelle is ~40 Å, which should be sufficient to avoid hydrophobic mismatch effects in a 24-residue (354–377) canonic helix. The higher flexibility of residues 366–369 observed in LPPG should therefore be considered a native attribute of the peptide.

Analysis of ^{15}N relaxation rates along the E1-TM backbone, in particular the elevated hetNOE values, defined the micelle-embedded segment of E1-TM between residues 354–378, encompassing the GxxxG motif and the two helical regions, with residue W353 lying at the solvent–micelle interface, a characteristic position for Trp residues. The global tumbling time of the E1-TM-LPPG assembly of 12 ns at 318 K is consistent with the expected size of a single peptide enclosed within an LPPG micelle. Measured R_2/R_1 ratios and solvent accessibility experiments along the membrane-spanning residues distinguished between the behavior of the H1 and H2 segments. The observed decreased transverse relaxation rates (Fig. 5) and lower solvent exchange protection factors (Fig. 6) in H1 residues are mutually consistent and indicative of increased internal motions in this region. Supporting this conclusion are the lower secondary chemical shifts observed for this helix (Fig. 4). It is important to note that the failure of the micelle to protect H1 amide protons from solvent exchange is not inconsistent with its localization within the micelle hydrophobic core. It has been shown that a glycine residue may facilitate exchange of neighboring amide protons with solvent, and that a sequence of 5–6 consecutive hydrophobic residues – as present in the H2 segment – is required for protection factors on the order of 10^3–10^5 [57,58]. In this context it is clear that the GxxxG motif, known for its involvement in inter-helical interactions in MPs [59], also greatly increases backbone flexibility, which may be necessary for binding to the E2 TM helix. Structural features of LPPG-embedded E1-TM as established in this study are summarized in Fig. 8.

Sidechains of basic amino acids located within membrane-spanning domains are known to 'snorkel', i.e. adopt a conformation which positions their methylene groups to contact the lipidic micelle interior while allowing their charged moiety to interact with negatively charged micelle headgroups [60,61]. It has been suggested that they serve to anchor TM-helices into a biologically-functional position within the membrane [62]. When considering the role of E1 residue K370 in glycoprotein heterodimerization, the presence of an oppositely charged residue (D728) in the E2 TM-domain is suggestive of formation of a membrane-embedded salt-bridge which would provide a strong driving force for association of the two peptides. In neutralizing this charge by mutation to alanine we hoped to mimic the effects of heterodimerization upon E1 conformation, and discovered that secondary structure was unchanged in the K370A mutant, suggesting that other inter-helical interactions

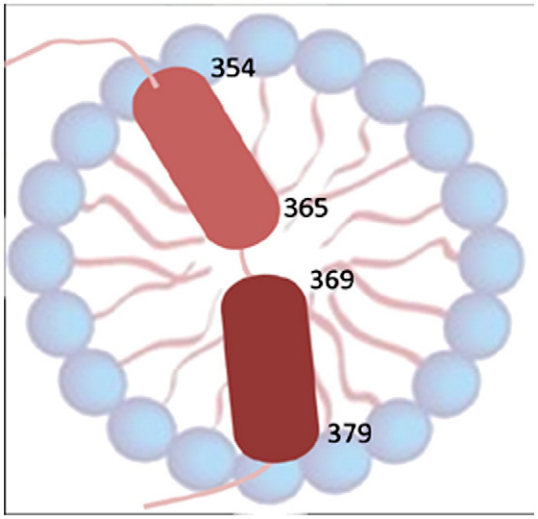

Fig. 8. Summary of NMR-derived global fold and motions of LPPG-embedded E1-TM. The E1-TM peptide (red) is schematically depicted within an LPPG micelle, with representative amino acid numbering. Helices and unstructured linkers appear in cylinders and lines, respectively. Backbone motions on the ps-ns timescale are color coded in the peptide sequence, with darker shades representing more rigid regions.

must be involved in structural changes accompanying glycoprotein heterodimerization. The changes observed in the fingerprint HSQC spectrum are reminiscent of the effects observed in a recent study of the β3 integrin lysine mutant, where a 'ripple' effect was observed for residues on one face of the TM helix [62]. This suggests that in the K370A mutant the helices relocate to a less polar region of the micelle interior, affecting the 'outer' side of the helix while exerting a smaller effect on its 'inner' side. Further studies are necessary to understanding the significance of this molecular event in the context of glycoprotein heterodimerization.

5. Conclusions

In conclusion, we have employed a combination of NMR methods to investigate the behavior of the E1 membrane-spanning domain in membrane-mimicking LPPG micelles, defining the overall size of the mixed micelle, the region embedded in the membrane, and the segments in the solubilized peptide adopting helical conformations. Besides demonstrating the power of NMR to characterize the biophysical behavior of membrane-spanning segments in the biologically important MPs, this study lays the foundation for future studies of E1/E2 association which may eventually contribute to a molecular understanding of this critical event in the life-cycle of HCV.

Acknowledgments

We gratefully acknowledge the ongoing support of Dr. Yoav Peleg (Weizmann Institute of Science, Rehovot, Israel) in design and cloning of E1-TM constructs, and thank Drs. Hugo Gottlieb and Keren Keinan-Adamsky and Mr. Israel Tabakman for technical support at the NMR facility. This work was supported in part by a research grant to J.H.C. by the Israel Science Foundation (801/09). The 700 MHz spectrometer was purchased with the support of the Converging Technologies Fund.

Appendix A. Supplementary data

Supplementary data to this article can be found online at http://dx.doi.org/10.1016/j.bbamem.2013.10.021.

References

[1] A. Craxi, G. Laffi, A.L. Zignego, Hepatitis C virus infection: a systemic disease, Mol. Asp. Med. 29 (2008) 85–95.
[2] B. Bartosch, F.-L. Cosset, Cell entry of hepatitis C virus, Virology 348 (2006) 1–12.
[3] D. Moradpour, F. Penin, Hepatitis C virus proteins: from structure to function, Curr. Top. Microbiol. Immunol. 369 (2013) 113–142.
[4] F. Poordad, V. Khungar, Emerging therapeutic options in hepatitis C virus infection, Am. J. Manage Care 17 (2011) S123–S130.
[5] A. Op De Beeck, C. Voisset, B. Bartosch, Y. Ciczora, L. Cocquerrel, Z. Keck, S. Foung, F.-L. Cosset, J. Dubuisson, Characterization of functional hepatitis C virus envelope glycoproteins, J. Virol. 78 (2004) 2994–3002.
[6] A. Wahid, F. Helle, V. Descamps, G. Duverlie, F. Penin, J. Dubuisson, Disulfide bonds in hepatitis C virus glycoprotein E1 control the assembly and entry functions of E2 glycoprotein, J. Virol. 87 (2013) 1605–1617.
[7] S. Rajesh, P. Sridhar, B.A. Tews, L. Fénéant, L. Cocquerel, D.G. Ward, F. Berditchevski, M. Overduin, Structural basis of ligand interactions of the large extracellular domain of tetraspanin CD81, J. Virol. 86 (2012) 9606–9616.
[8] J. Fraser, I. Boo, P. Poumbourios, H.E. Drummer, Hepatitis C virus (HCV) envelope glycoproteins E1 and E2 contain reduced cysteine residues essential for virus entry, J. Biol. Chem. 286 (2012) 31984–31992.
[9] E. Falkowska, F. Kajumo, E. Garcia, J. Reinus, T. Dragic, Hepatitis C virus envelope glycoprotein E2 glycans modulate entry, CD81 binding, and neutralization, J. Virol. 81 (2007) 8072–8079.
[10] M.J. Farquhar, H.J. Harris, J.A. McKeating, Hepatitis C virus entry and the tetraspanin CD81, Biochem. Soc. Trans. 39 (2011) 532–536.
[11] G.A. Sautto, R.A. Diotti, M. Clementi, New therapeutic options for HCV infection in the monoclonal antibody era, New Microbiol. 35 (2012) 387–397.
[12] A. Op De Beeck, J. Dubuisson, Topology of hepatitis C virus envelope glycoproteins, Rev. Med. Virol. 13 (2003) 233–241.
[13] Y. Ciczora, N. Callens, C. Montpellier, B. Bartosch, F.-L. Cosset, A. Op De Beeck, J. Dubuisson, Contribution of the charged residues of hepatitis C virus glycoprotein E2 transmembrane domain to the functions of the E1 E2 heterodimer *J*, Gen. Virol. 86 (2005) 2793–2798.
[14] Y. Ciczora, N. Callens, F. Penin, E.-I. Pecheur, J. Dubuisson, Transmembrane domains of hepatitis C virus envelope glycoproteins: residues involved in the E1E2 heterodimerization and involvement of these domains in virus entry, J. Virol. 81 (2007) 2372–2381.
[15] H. Yin, Exogenous agents that target transmembrane domains of proteins, Angew. Chem. Int. Ed. 47 (2008) 2744–2752.
[16] L. Fagerberg, K. Jonasson, G. von Heijne, M. Uhlen, L. Berglund, Prediction of the human membrane proteome, Proteomics 10 (2010) 1141–1149.
[17] N. Bordag, S. Keller, Alpha-helical transmembrane peptides: a "divide and conquer" approach to membrane proteins, Chem. Phys. Lipids 163 (2010) 1–26.
[18] P. Hubert, P. Sawma, J.P. Duneau, J. Khao, J. Henin, D. Bagnard, J. Sturgis, Single-spanning transmembrane domains in cell growth and cell-cell interactions: more than meets the eye? Cell Adhes. Migr. 4 (2010) 313–324.
[19] E.V. Bocharov, P.E. Volynsky, K.V. Pavlov, R.G. Efremov, A.S. Arseniev, Structure elucidation of dimeric transmembrane domains of bitopic proteins, Cell Adhes. Migr. 4 (2010) 284–298.
[20] T. Qureshi, N.K. Goto, Contemporary methods in structure determination of membrane proteins by solution NMR, Top. Curr. Chem. 326 (2012) 123–185.
[21] A. Arora, L.K. Tamm, Biophysical approaches to membrane protein structure determination, Curr. Opin. Struct. Biol. 11 (2001) 540–547.
[22] R.D. Krueger-Koplin, P.L. Sorgen, S.T. Krueger-Koplin, I.O. Rivera-Torres, S.M. Cahill, D.B. Hicks, L. Grinius, T.A. Krulwich, M.E. Girvin, An evaluation of detergents for NMR structural studies of membrane proteins, J. Biomol. NMR 28 (2004) 43–57.
[23] R.C. Page, J.D. Moore, H.B. Nguyen, M. Sharma, R. Chase, F.P. Gao, C.K. Mobley, C.R. Sanders, L. Ma, F.D. Sonnichsen, S. Lee, S.C. Howell, S.J. Opella, T.A. Cross, Comprehensive evaluation of solution nuclear magnetic resonance spectroscopy sample preparation for helical integral membrane proteins, J. Struct. Func. Genom. 7 (2006) 51–64.
[24] D. Warschawski, A.A. Arnold, M. Beaugrand, A. Gravel, E. Chartrand, I. Marcotte, Choosing membrane mimetics for NMR structural studies of transmembrane proteins, Biochim. Biophys. Acta 1808 (2009) 1957–1974.
[25] F. Hagn, M. Etzkorn, T. Raschle, G. Wagner, Optimized phospholipid bilayer nanodiscs facilitate high-resolution structure determination of membrane proteins, J. Am. Chem. Soc. 135 (2013) 1919–1925.
[26] A.G. Palmer, III, C.D. Kroenke, J.P. Loria, Nuclear magnetic resonance methods for quantifying microsecond-to-millisecond motions in biological macromolecules, Methods Enzymol. 339 (2001) 204–238.
[27] G.M. Clore, C. Tang, J. Iwahara, Elucidating transient molecular interactions using paramagnetic relaxation enhancement, Curr. Opin. Struct. Biol. 17 (2007) 603–616.
[28] K.J. Walters, A.E. Ferentz, B.J. Hare, P. Hidalgo, A. Jasanoff, H. Matsuo, G. Wagner, Characterizing protein-protein complexes and oligomers by nuclear magnetic resonance spectroscopy, Methods Enzymol. 339 (2001) 238–258.
[29] L. Columbus, W.L. Hubbell, A new spin on protein dynamics, Trends Biochem. Sci. 27 (2002) 288–295.
[30] H. Takahashi, T. Nakanishi, K. Kami, Y. Arata, I. Shimada, A novel NMR method for determining the interfaces of large protein-protein complexes, Nat. Struct. Biol. 7 (2000) 220–223.
[31] E.R.P. Zuiderweg, Mapping protein-protein interactions in solution by NMR spectroscopy, Biochemistry 41 (2003) 1–7.
[32] T. Zhuang, B.K. Jap, C.R. Sanders, Solution NMR approaches for establishing specificity of weak heterodimerization of membrane proteins, J. Am. Chem. Soc. 133 (2011) 20571–20580.
[33] L.E. Kay, NMR studies of protein structure and dynamics, J. Magn. Reson. 173 (2005) 193–207.
[34] M. Cai, Y. Huang, K. Sakaguchi, G.M. Clore, A.M. Gronenborn, R. Craigie, An efficient and cost-effective isotope labeling protocol for proteins expressed in Escherichia coli, J. Biomol. NMR 11 (1998) 97–102.
[35] Y. Peleg, T. Unger, Application of high-throughput methodologies to the expression of recombinant proteins in E. coli, Methods Mol. Biol. 426 (2008) 197–208.
[36] T. Unger, Y. Jacobovitch, A. Dantes, R. Bernheim, Y. Peleg, Applications of the Restriction Free (RF) cloning procedure for molecular manipulations and protein expression, J. Struct. Biol. 172 (2010) 34–44.
[37] L. Whitmore, B.A. Wallace, Protein secondary structure analyses from circular dichroism spectroscopy: methods and reference databases, Biopolymers 89 (2004) 392–400.
[38] M. Salzmann, G. Wider, K. Pervushin, H. Senn, K. Wuthrich, TROSY-type triple-resonance experiments for sequential NMR assignments of large proteins, J. Am. Chem. Soc. 121 (1999) 844–848.
[39] A.G. Palmer III, NMR probes of molecular dynamics: overview and comparison with other techniques, Annu. Rev. Biophys. Biomol. Struct. 30 (2001) 129–155.
[40] J.G. Kempf, J.P. Loria, Protein dynamics from solution NMR: theory and applications, Cell Biochem. Biophys. 37 (2003) 187–211.
[41] D. Lavillette, E.I. Pecheur, P. Donot, J. Fresquet, J. Molle, R. Corbau, M. Dreux, F. Penin, F.L. Cosset, Characterization of fusion determinants points to the involvement of three discrete regions of both E1 and E2 glycoproteins in the membrane fusion process of hepatitis C virus, J. Virol. 81 (2007) 8752–8765.
[42] A.J. Perez-Berna, A. Bernabeu, M.R. Moreno, J. Guillen, J. Villalain, The pre-transmembrane region of the HCV E1 glycoprotein: interaction with model membranes, Biochim. Biophys. Acta 1778 (2008) 2069–2080.
[43] A.J. Perez-Berna, M.R. Moreno, J. Guillen, A. Bernabeu, J. Villalain, The membrane-active regions of the hepatitis C virus E1 and E2 envelope glycoproteins, Biochemistry 45 (2006) 3755–3768.
[44] R. Spadaccini, G. D'Errico, V. D'Alessio, E. Notomista, A. Bianchi, M. Merola, D. Picone, Structural characterization of the transmembrane proximal region of the hepatitis C virus E1 glycoprotein, Biochim. Biophys. Acta Biomembr. 1798 (2010) 344–353.
[45] P. Sun, J.E. Tropea, D.S. Waugh, Enhancing the solubility of recombinant proteins in Escherichia coli by using hexahistidine-tagged maltose-binding protein as a fusion partner, Methods Mol. Biol. 705 (2011) 259–274.
[46] C.R. Sanders, F.D. Sonnichsen, Solution NMR of membrane proteins: practice and challenges, Magn. Reson. Chem. 44 (2006) S24–S40.

[47] O. Vinogradova, F.D. Sonnichsen, C.R. Sanders, On choosing a detergent for solution NMR studies of membrane proteins, J. Biomol. NMR 11 (1998) 381–386.
[48] C. Camilloni, A. De Simone, W.F. Vranken, M. Vendruscolo, Determination of secondary structure populations in disordered states of proteins using nuclear magnetic resonance chemical shifts, Biochemistry 51 (2012) 2224–2231.
[49] F. Ferrage, Protein dynamics by ^{15}N nuclear magnetic relaxation, Methods Mol. Biol. 831 (2012) 141–163.
[50] J.J. Chou, J.L. Baber, A. Bax, Characterization of phospholipid mixed micelles by translational diffusion, J. Biomol. NMR 29 (2003) 299–308.
[51] D.E. Woessner, Nuclear spin relaxation in ellipsoids undergoing rotational Brownian motion, J. Chem. Phys. 37 (1962) 647–654.
[52] J.M. Schurr, H.P. Babcock, B.S. Fujimoto, A test of the model-free formulas – effects of anisotropic rotational diffusion and dimerization, J. Magn. Reson. Ser. B 105 (1994) 211–224.
[53] Y. Bai, J.S. Milne, L. Mayne, S.W. Englander, Primary structure effects on peptide group hydrogen exchange, Proteins 17 (1993) 75–86.
[54] M. Itaya, I.C. Brett, S.O. Smith, Synthesis, purification, and characterization of single helix membrane peptides and proteins for NMR spectroscopy, Methods Mol. Biol. 831 (2012) 333–357.
[55] A. Meruelo, I. Samish, J.U. Bowie, TMKink: a method to predict transmembrane helix kinks, Prot. Sci. 20 (2011) 1256–1264.
[56] U.H. Dürr, M. Gildenberg, A. Ramamoorthy, The magic of bicelles lights up membrane protein structure, Chem. Rev. 112 (2012) 6054–6074.
[57] J.H. Chill, J.M. Louis, C. Miller, A. Bax, NMR study of the tetrameric KcsA potassium channel in detergent micelles, Prot. Sci. 15 (2006) 684–698.
[58] J.H. Chill, J.M. Louis, F. Delaglio, A. Bax, Local and global structure of the monomeric subunit of the potassium channel KcsA probed by NMR, Biochim. Biophys. Acta 1768 (2007) 3260–3270.
[59] A. Senes, D.E. Engel, W.F. DeGrado, Folding of helical membrane proteins: the role of polar, GxxxG-like and proline motifs, Curr. Opin. Struct. Biol. 14 (2004) 465–479.
[60] A.K. Chamberlain, Y. Lee, S. Kim, J.U. Bowie, Snorkeling preferences foster an amino acid composition bias in transmembrane helices, J. Mol. Biol. 339 (2004) 471–479.
[61] E. Strandberg, J.A. Killian, Snorkeling of lysine side chains in transmembrane helices: how easy can it get? FEBS Lett. 544 (2003) 69–73.
[62] C. Kim, T. Schmidt, E.G. Cho, F. Ye, T.S. Ulmer, M.H. Ginsberg, Basic amino-acid side chains regulate transmembrane integrin signalling, Nature 481 (2012) 209–213.